AMERICAN SOCIETY FOR MICROBIOLOGY | mBio®

OBSERVATION

Structural Basis for Linezolid Binding Site Rearrangement in the *Staphylococcus aureus* Ribosome

Matthew J. Belousoff,[a] Zohar Eyal,[b] Mazdak Radjainia,[c] Tofayel Ahmed,[d] Rebecca S. Bamert,[a] Donna Matzov,[b] Anat Bashan,[b] Ella Zimmerman,[b] Satabdi Mishra,[d] David Cameron,[a] Hans Elmlund,[c,e] Anton Y. Peleg,[a,f] Shashi Bhushan,[d,g] Trevor Lithgow,[a] Ada Yonath[b]

Infection & Immunity Program, Biomedicine Discovery Institute & Department of Microbiology, Monash University, Clayton, Australia[a]; Department of Structural Biology, Weizmann Institute of Science, Rehovot, Israel[b]; The Clive and Vera Ramaciotti Centre for Structural Cryo-Electron Microscopy, Department of Biochemistry and Molecular Biology, Monash University, Victoria, Melbourne, Australia[c]; School of Biological Sciences, Nanyang Technological University, Singapore, Singapore[d]; Infection & Immunity Program, Biomedicine Discovery Institute & Department of Biochemistry and Molecular Biology, Monash University, Clayton, Australia[e]; Department of Infectious Diseases, Alfred Hospital, Prahran, Australia[f]; NTU Institute of Structural Biology, Nanyang Technological University, Singapore, Singapore[g]

ABSTRACT An unorthodox, surprising mechanism of resistance to the antibiotic linezolid was revealed by cryo-electron microscopy (cryo-EM) in the 70S ribosomes from a clinical isolate of *Staphylococcus aureus*. This high-resolution structural information demonstrated that a single amino acid deletion in ribosomal protein uL3 confers linezolid resistance despite being located 24 Å away from the linezolid binding pocket in the peptidyl-transferase center. The mutation induces a cascade of allosteric structural rearrangements of the rRNA that ultimately results in the alteration of the antibiotic binding site.

IMPORTANCE The growing burden on human health caused by various antibiotic resistance mutations now includes prevalent *Staphylococcus aureus* resistance to last-line antimicrobial drugs such as linezolid and daptomycin. Structure-informed drug modification represents a frontier with respect to designing advanced clinical therapies, but success in this strategy requires rapid, facile means to shed light on the structural basis for drug resistance (D. Brown, Nat Rev Drug Discov 14:821–832, 2015, https://doi.org/10.1038/nrd4675). Here, detailed structural information demonstrates that a common mechanism is at play in linezolid resistance and provides a step toward the redesign of oxazolidinone antibiotics, a strategy that could thwart known mechanisms of linezolid resistance.

KEYWORDS staphylococcus, antibiotic resistance, ribosomal mutations

Received 27 March 2017 **Accepted** 17 April 2017 **Published** 9 May 2017

Citation Belousoff MJ, Eyal Z, Radjainia M, Ahmed T, Bamert RS, Matzov D, Bashan A, Zimmerman E, Mishra S, Cameron D, Elmlund H, Peleg AY, Bhushan S, Lithgow T, Yonath A. 2017. Structural basis for linezolid binding site rearrangement in the *Staphylococcus aureus* ribosome. mBio 8:e00395-17. https://doi.org/10.1128/mBio.00395-17.

Invited Editor Gongyi Zhang, National Jewish Hospital

Editor Robert A. Bonomo, Louis Stokes Veterans Affairs Medical Center

Address correspondence to Trevor Lithgow, trevor.lithgow@monash.edu, or Ada Yonath, ada.yonath@weizmann.ac.il.

M.J.B., Z.E., and M.R. contributed equally to this article.

Ribosomes (Fig. 1a) are the cellular nanomachines responsible for protein synthesis (1, 2). As such, the bacterial ribosome is targeted by over 40% of the antibiotics (3) in clinical use. While the acquisition of resistance to many of these antibiotics is of great current concern, two strategies stand out for clinically relevant "push back" at drug resistance phenotypes: (i) the design of novel antibiotics and (ii) the use of structure-informed drug engineering to modify current antibiotics to produce variant antibiotics by pinpointing and then overcoming steric factors in drug-resistant ribosomes (4). Linezolid—the first fully synthetic antibiotic—was introduced as a new drug in the clinic in 2000 (5, 6). It inhibits bacterial protein synthesis by binding in the peptidyl transferase center (PTC), the active site of the large 50S ribosomal subunit (Fig. 1b). Linezolid binding leads to steric hinderance that selectively modulates tRNA binding into the A-site of the ribosome (7, 8), and crystal structures reveal that the bound

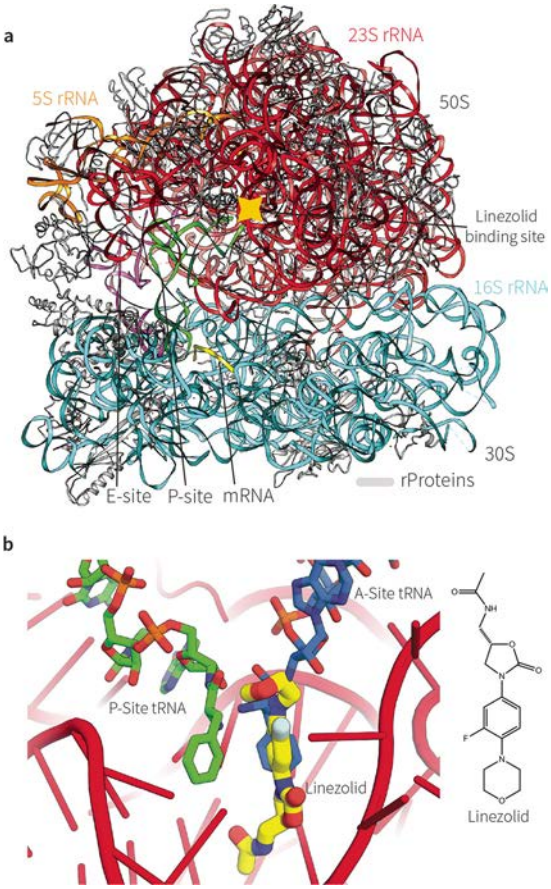

FIG 1 Linezolid binding and protein synthesis in *S. aureus*. (a) The overall structure of the 70S ribosome from *S. aureus* (Lin^S). (b) (Left panel) The 23S rRNA of the catalytic site is shown in red, the amino-acylated end of the A-site tRNA is shown in green, and the P-site tRNA is shown in orange. The antibiotic linezolid, overlapping the position that the A-site tRNA would otherwise occupy, is shown in yellow. Upon linezolid binding, no amino-acylated tRNAs can enter the active site and form new peptide bonds. The cartoon represents a composite of two PDB entries: 4WFA (24) and 4V5D (38). (Right panel) The chemical structure of linezolid.

linezolid adopts similar orientations in the A-sites of ribosomes from bacterial species as diverse as *Deinococcus radiodurans*, *Haloarcula marismortui*, *Staphylococcus aureus*, and *Escherichia coli* (9).

The acquisition of linezolid resistance by methicillin-resistant *Staphylococcus aureus* (MRSA) is now of global concern (10–12). In the absence of new antibiotics, reengineering of a drug like linezolid is potentially an attractive strategy (4). In terms of genome-based characterization, resistance to linezolid is conferred by numerous rRNA mutations, with particular prevalence seen in the mutations C^{2576}U, U^{2500}A, C^{2190}U, and G^{2603}U (*E. coli* 23S rRNA numbering is used throughout) (10, 13–16) and in the acquisition by lateral transfer of the *cfr* gene encoding a methyltransferase that modifies A^{2503} in the 23S rRNA. Strains of MRSA with the combination of G^{2603}U and the *cfr* gene are now of particular concern in Asia (10). Seemingly at odds with the observation that a discrete set of rRNA mutations are causative for linezolid resistance, a recent increase in the levels of isolates of linezolid-resistant pathogens, including MRSA, with mutations in ribosomal protein uL3, a ribosomal protein positioned at a location distant from that of the PTC, has been reported (15, 17). To rationalize these observations, current biochemically based hypothetical models suggest various sterically different solutions to resist linezolid binding (15, 18). A scenario such as this, with various structurally distinct mechanisms at play, would make unfeasible any attempt to reengineer a form of linezolid that could reliably act against linezolid-resistant pathogens.

We examined a linezolid-resistant (Lin^r) clinical isolate of MRSA from an Australian hospital by single-particle cryo-electron microscopy (cryo-EM). The antibiotic susceptibility of the strain was assessed by *in vitro* transcription-translation assays using bacterial cell extracts. These data quantify susceptibility to inhibition of translation, with ribosomes from the Lin^r strain showing a more than 4-fold increase in the 50% inhibitory concentration (IC_{50}) compared to ribosomes from the type (Lin^s) strain, ATCC 35556 (Fig. 2a). Genome sequencing of the Lin^r strain revealed that linezolid resistance was due not to the presence of the *cfr* gene or to any mutation in the rRNA genes but to the presence of a single amino acid deletion (Δ^{S145}) in ribosomal protein (rProtein) uL3 (see Fig. S1 in the supplemental material). The mutation in uL3 sits at a location greatly distal to the PTC (>20 Å away), and we sought to use high-resolution structural data to reconcile the architectural constraints in the ribosome with the drug resistance phenotype.

Using a rapid workflow for cryo-EM data acquisition and data processing, single-particle reconstructions enabled determination of 70S ribosome structures from the Lin^s and Lin^r strains of *S. aureus* (Fig. S2, Fig. S3, Table S1). Ribosomes were extracted from cultures at mid-log phase and purified from bacterial cell extracts by ultracentrifugation coupled with hydrophobic interaction chromatography and sucrose gradient fractionation (see Text S1 in the supplemental material). At the time of this study, no high-resolution structural data were available for 70S ribosomes from *S. aureus*. Processing of the raw cryo-EM data was performed with RELION software (19), resulting in a 3.9-Å map of the 70S ribosome from the Lin^s strain and a 3.6-Å resolution map of the Lin^r 70S ribosome (Fig. S4). The structures were solved initially using a low-resolution 70S model that was built by the use of structure threading protocols in the Rosetta software suite (20), followed by manual loop building. Next, the model was fitted to the electron density maps using guided molecular dynamic simulations as implemented in NAMD2 (21) (Fig. S3). Bond geometry optimization and the final molecular refinement were carried out in real space using the PHENIX software package (22). The accuracy of the resulting atomic models was judged by an all-atom comparison to the recent X-ray crystal structure of the 50S subunit from the *S. aureus* ribosome (PDB 4WCE). This validation experiment showed the accuracy of the cryo-EM data processing, given a root mean square deviation (RMSD) of less than 0.5 Å.

While the data have not yet been released, a recent paper by Yusupov, Hashem, and coworkers describes in detail unique features of the Lin^s 70S ribosome from *S. aureus* (23). In relation to that structure, our results provide the first comparison of ribosomes from Lin^s and Lin^r; hence, the analysis presented here focuses on the mechanism of linezolid resistance. The ribosomes from Lin^s and Lin^r differ by a large structural rearrangement in loop 6 of uL3 (Fig. 2b; Fig. S5a). The deletion of Ser145 induced a contraction of the rProtein loop, while most interactions with helix 90 in the 23S rRNA were retained (Fig. 2b).

This dragged the rRNA helix away from the PTC (by ~2 Å), leading to noticeable differences in the architecture of the linezolid binding site (Fig. 2b and d). Comparing the Lin^r and Lin^s structures revealed a large shift in G^{2505} into the binding site of linezolid (Fig. 2e). This shift was mediated by the change in orientation of G^{2581} in helix 90 due to the change in uL3. This structural shift completely remodeled the linezolid binding cavity (Fig. 2e) and removed a critical hydrogen bond between the ribose backbone (G^{2505}) and the 2-oxazolidone moiety of the antibiotic (24), explaining the lower binding efficacy of the drug.

Further structure comparison also revealed subtler differences in rearrangements of the rRNA base orientations in the PTC (Fig. S5b). The rRNA bases undergoing the largest shifts are U^{2504}, G^{2505}, U^{2506}, G^{2576}, and U^{2584}, all of which either are within or surround the PTC. In other Lin^r strains, these bases are common targets for the mutations that directly confer linezolid resistance (Fig. S5c). Our work demonstrates how a clinically relevant mutation in uL3, which is located more than 20 Å away from the drug pocket, propagates alterations through to these rRNA residues surrounding the linezolid binding site. This link between the ΔSer145 mutation in uL3 and mutations in the 23S rRNA

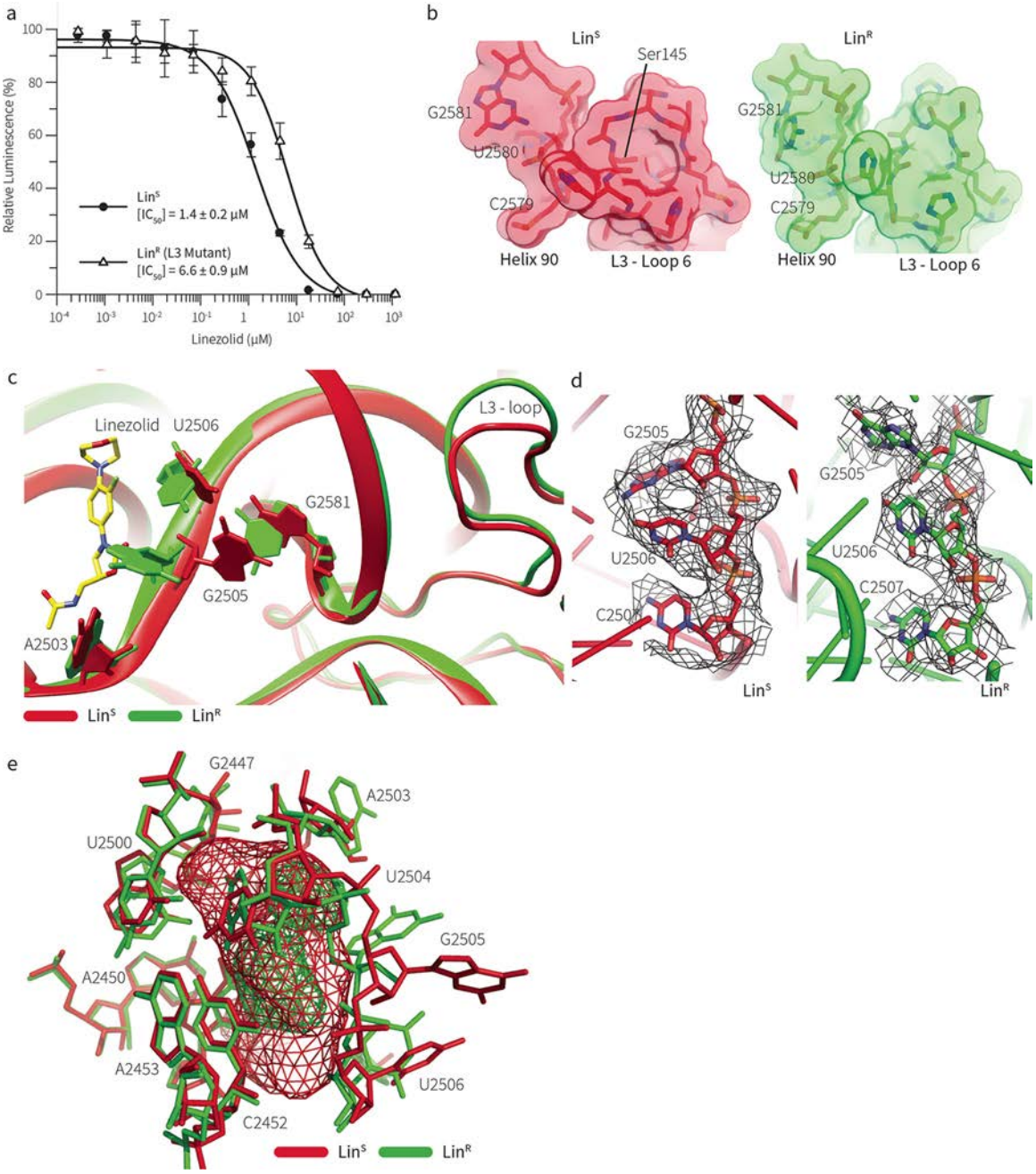

FIG 2 A structural clash that prevents linezolid binding in Lin^r MRSA. (a) *In vitro* (IC_{50}) cell-free transcription-translation assay. Data are plotted as the amount of protein synthesis (measured by luciferase translation) versus the concentration of linezolid (in micrograms per milliliter). (b) Representation of the region of uL3 around the site of the ΔSer145 mutation, viewed in the same orientation. The Lin^s structure is shown on the left (red); the Lin^r structure is shown on the right (green). The portion of uL3 that interacts with rRNA in "helix 90" is shown. The Lin^r structure reveals a contraction in the loop of uL3, visible here by the repositioning of His146 (uL3) to become His145 (uL3) in the LinR ribosome, altering the interaction of this loop with helix 90 of the 23S rRNA. (c) The cryo-EM structure of the 70S ribosome from Lin^s, showing the linezolid position (yellow) and its interaction with 23S rRNA nucleotide G^{2505} (the position of linezolid is from PDB 4WFA). The cryo-EM structure of the 70S ribosome from Lin^r is overlaid in green. Deletion of a single amino acid in the uL3 rProtein of the Lin^r ribosome changes the part of the protein that interacts with an rRNA helix, a helix which in turn makes a direct contact with linezolid. This structural change modifies the position of G^{2505} in the drug binding pocket, contracting this region and providing fewer contacts to stabilize drug binding. (d) Electron density (drawn at 3σ) around the rRNA nucleotides closest to the linezolid binding site in both the Lin^s (red, left panel) and Lin^r (green, right panel), showing the change in orientation of these nucleotides due to the mutation in uL3. (e) Overlay of the cryo-EM structures of the Lin^s and Lin^r 70S ribosomes around the binding cavity of the linezolid antibiotic. The cavity available for linezolid binding is shown in the colored mesh. The remodeled Lin^r binding site (green) is more constricted and less permissive of linezolid binding.

leads to the suggestion that, to achieve a linezolid resistance phenotype, staphylococci must acquire a common spatial change in the linezolid binding site. This common architectural deviation in the various linezolid-resistant mutants provides both an experimental framework and a confidence to engage in drug engineering.

Methods. More-detailed descriptions of the methods used are available in the supplemental material. All figures were generated with either Pymol (25) or UCSF Chimera (26).

MIC and IC_{50} assays. MIC assays were carried out according to the established protocol as described by Andrews (27). Strains were cultured and assayed for antibiotic inhibition in cation-adjusted Mueller-Hinton broth. IC_{50} assays were performed as previously described (28). Briefly, the inhibition effect of linezolid on *S. aureus* ribosomes was tested in a bacterial coupled transcription/translation assay system which measures the expression of the luciferase gene (29). The results were plotted, and IC_{50} values were calculated with the GraFit software package (30).

Genome sequencing. Genomic DNA was isolated from overnight cultures using a Qiagen genomic DNA (gDNA) kit. The DNA was then subjected to DNA library preparation following the protocols outlined by Illumina. Short-read DNA sequencing reads (150 bases, paired ends) were collected on an Illumina MiSeq sequencer and assembled in the Geneious software package.

Ribosome isolation. (i) Lin^s 70S ribosomes with tRNA and mRNA (Lin^s). *S. aureus* RN4220 (American Type Culture Collection 35556) (31) was grown and disrupted, and the ribosomes were isolated as described previously (24). Ribosome samples were kept in buffer (10 mM HEPES [pH 7.6], 10 mM $MgCl_2$, 60 mM NH_4Cl, 15 mM KCl) and brought to a final concentration of not higher than 1,000 $A_{260} \cdot ml^{-1}$ and then were flash-frozen for storage at −80°C.

(ii) Apo-Lin^r 70S ribosomes (Lin^r). *S. aureus* bacteria (clinical isolate from Alfred Hospital, Melbourne, Australia) were incubated overnight in 5-ml cultures of brain heart infusion broth. After subculture into 4.5 liters of brain heart infusion broth and growth at 37°C until an optical density (600 nm) of 1.5 was reached, cells were harvested by centrifugation and washed in a buffer containing 10 mM Tris-acetate (pH = 8.0), 14 mM magnesium acetate ($MgAc_2$), 50 mM KCl, and 1 mM dithiolthreitol (DTT). Cell pellets were flash-frozen with liquid N_2. Frozen cell pellets were thawed in the presence of a buffer containing 10 mM Tris-acetate (pH = 8.0), 20 mM $MgAc_2$, 50 mM KCl, and 1 mM DTT. Lysostaphin (80 μg/ml) and DNase I (80 μg/ml) were added to this solution. This cell slurry was incubated at 37°C for 30 min before emulsification was performed using an Avestin Emulsiflex C3 homogenizer. The cell lysate was clarified by centrifugation (45,000 relative centrifugal force [RCF], 30 min, 4°C), and the crude ribosome particles were collected from the clarified lysate by ultracentrifugation into a sucrose cushion (230,000 RCF, 19 h, 4°C). The crude ribosome pellet was suspended in buffer containing 1.5 M $(NH_4)_2SO_4$, 20 mM $MgAc_2$, 400 mM KCl, and 20 mM Tris-acetate (pH = 8.0). This solution was then subjected to hydrophobic interaction chromatography using 650 M butyl resin. 70S ribosomes were eluted over a linear ammonium sulfate gradient. Fractions containing 70S particles were pooled and pelleted by ultracentrifugation (230,000 RCF, 19 h, 4°C). The resulting clear pellet was resuspended in a buffer containing 20 mM Tris-acetate (pH = 8.0), 15 mM $MgAc_2$, 50 mM KCl, and 10% (wt/vol) sucrose. This mixture was then subjected to sucrose gradient centrifugation across a linear gradient spanning 10% to 40% (wt/vol) sucrose. Fractions eluted from the sucrose gradient containing pure 70S ribosomes were pooled and dialyzed against a buffer containing 20 mM HEPES (pH = 7.4), 15 mM $MgAc_2$, 50 mM KAc, 10 mM NH_4Ac, and 0.5 mM DTT. These purified ribosomes were generally at a suitable concentration for immediate application to the transmission electron microscopy (TEM) grids (~300 ng/μl).

Electron microscopy. Samples (4 to 5 μl) were applied to a glow-discharged Quantifoil holey carbon grid (Quantifoil GmbH, Großlöbichau, Germany) and were flash-frozen in liquid ethane using an FEI Vitrobot system (FEI, Hillsboro, OR). Data for

the Lin^s ribosome were collected on a Tecnai Arctica FEI EM operating at 200-kV acceleration voltage and at a nominal level of underfocus ($\Delta z = -1$ to -2.7 μm) using a second-generation complementary metal oxide semiconductor (CMOS) back-thinned direct electron detector (Falcon II) 4,096-by-4,096-pixel camera with a calibrated magnification of $\times$110,000, corresponding to 0.96 Å per pixel at the specimen level. Exposure time was 1.5 s with a dose of 40 e $\cdot$ Å^{-2}. Data for the Lin^r ribosome were collected on an FEI Titan Krios EM operating at 300-kV acceleration voltage at defocus values similar to those employed with the Lin^s sample and using the same electron detector. The calibrated magnification was $\times$127,000, corresponding to 1.1 Å per pixel at the specimen level. Exposure time was 1 s with a dose of 45 e $\cdot$ Å^{-2}.

Data processing. Movies were integrated with EMAN (32) or UCSF MotionCor2 (33), and CTF estimation was performed with CTFFIND3 (34). Particles were picked from the micrographs using EMAN (32), and particle analysis and final three-dimensional (3D) reconstruction were performed using RELION (19).

Atomic model refinement. A model of the *S. aureus* 70S ribosome was created using an *E. coli* 70S model (3J9Z) (35). This was achieved using the RNA threading protocol in the Rosetta software package (20) for generating the rRNA and the Sculptor (22) application in the PHENIX software package combined with loop modeling as implemented in coot (36). The resulting model was then subjected to energy minimization in order to remove any steric clashes. Fitting the model to the cryo-EM electron density map was achieved using the MDFF routine in namd (37). The fitted model was further refined by rounds of manual model building in coot (36) and real-space refinement as implemented in the Phenix software package (22).

Accession number(s). The structures were deposited with accession codes PDB 5T7V and EMDB EMD-8369 (Lin^r) and accession codes PDB 5TCU and EMDB EMD-8402 (Lin^s).

SUPPLEMENTAL MATERIAL

Supplemental material for this article may be found at https://doi.org/10.1128/mBio.00395-17.

TEXT S1, PDF file, 0.1 MB.
TABLE S1, PDF file, 0.1 MB.
FIG S1, PDF file, 0.4 MB.
FIG S2, PDF file, 0.7 MB.
FIG S3, PDF file, 1 MB.
FIG S4, PDF file, 1.4 MB.
FIG S5, PDF file, 0.7 MB.

ACKNOWLEDGMENTS

We thank Georg Ramm for Titan Krios support and Ashley Buckle for the use of the ORCHARD computation cluster used for the NAMD calculations. We thank Susanne Paukner and Rosemarie Riedl of Nabriva Therapeutics AG, Vienna, Austria, for Lin^s growth. We thank Moran Ben-Ami, Shoshana Tel-Or, Miriam Lachever, and Maggie Kessler for their interest and experimental support. We acknowledge the Nvidia Corporation for donating GPUs to aid with calculations used in this research.

This work was supported by the Multi-modal Australian Sciences Imaging and Visualization Environment (MASSIVE) (http://www.massive.org.au). Funding was provided by European Research Council grant 322581 (NOVRIB), the National Health & Medical Research Council of Australia (Program grant 1092262), and the Kimmelman Center for Macromolecular Assemblies. M.J.B. is an NHMRC Postdoctoral Fellow; T.L. is an Australian Research Council Laureate Fellow; A.Y. holds the Martin S. and Helen Kimmel Professorial Chair at the Weizmann Institute of Science. The funders had no role in study design, data collection and interpretation, or the decision to submit the work for publication.

REFERENCES

1. Bashan A, Agmon I, Zarivach R, Schluenzen F, Harms J, Berisio R, Bartels H, Franceschi F, Auerbach T, Hansen HA, Kossoy E, Kessler M, Yonath A. 2003. Structural basis of the ribosomal machinery for peptide bond formation, translocation, and nascent chain progression. Mol Cell 11:91–102. https://doi.org/10.1016/S1097-2765(03)00009-1.
2. Ramakrishnan V. 2002. Ribosome structure and the mechanism of translation. Cell 108:557–572. https://doi.org/10.1016/S0092-8674(02)00619-0.
3. Poehlsgaard J, Douthwaite S. 2005. The bacterial ribosome as a target for antibiotics. Nat Rev Microbiol 3:870–881. https://doi.org/10.1038/nrmicro1265.
4. Brown D. 2015. Antibiotic resistance breakers: can repurposed drugs fill the antibiotic discovery void? Nat Rev Drug Discov 14:821–832. https://doi.org/10.1038/nrd4675.
5. Brickner SJ, Barbachyn MR, Hutchinson DK, Manninen PR. 2008. Linezolid (ZYVOX), the first member of a completely new class of antibacterial agents for treatment of serious gram-positive infections. J Med Chem 51:1981–1990. https://doi.org/10.1021/jm800038g.
6. Leach KL, Brickner SJ, Noe MC, Miller PF. 2011. Linezolid, the first oxazolidinone antibacterial agent. Ann N Y Acad Sci 1222:49–54. https://doi.org/10.1111/j.1749-6632.2011.05962.x.
7. Marks J, Kannan K, Roncase EJ, Klepacki D, Kefi A, Orelle C, Vázquez-Laslop N, Mankin AS. 2016. Context-specific inhibition of translation by ribosomal antibiotics targeting the peptidyl transferase center. Proc Natl Acad Sci U S A 113:12150–12155. https://doi.org/10.1073/pnas.1613055113.
8. Du Toit A. 2016. Antimicrobials: putting antibiotic action into context. Nat Rev Microbiol 14:725. https://doi.org/10.1038/nrmicro.2016.165.
9. Wilson DN. 2014. Ribosome-targeting antibiotics and mechanisms of bacterial resistance. Nat Rev Microbiol 12:35–48. https://doi.org/10.1038/nrmicro3155.
10. Zhou W, Niu D, Cao X, Ning M, Zhang Z, Shen H, Zhang K. 2015. Clonal dissemination of linezolid-resistant Staphylococcus capitis with G2603T mutation in domain V of the 23S rRNA and the cfr gene at a tertiary care hospital in China. BMC Infect Dis 15:97. https://doi.org/10.1186/s12879-015-0841-z.
11. Balandin B, Lobo B, Orden B, Román F, García E, Martínez R, Valdivia M, Ortega A, Fernández I, Galdos P. 2016. Emergence of linezolid-resistant coagulase-negative staphylococci in an intensive care unit. Infect Dis 48:343–349. https://doi.org/10.3109/23744235.2015.1122225.
12. Cafini F, Nguyen LTT, Higashide M, Román F, Prieto J, Morikawa K. 2016. Horizontal gene transmission of the cfr gene to MRSA and enterococcus: role of Staphylococcus epidermidis as a reservoir and alternative pathway for the spread of linezolid resistance. J Antimicrob Chemother 71:587–592. https://doi.org/10.1093/jac/dkv391.
13. Tsiodras S, Gold HS, Sakoulas G, Eliopoulos GM, Wennersten C, Venkataraman L, Moellering RC, Ferraro MJ. 2001. Linezolid resistance in a clinical isolate of Staphylococcus aureus. Lancet 358:207–208. https://doi.org/10.1016/S0140-6736(01)05410-1.
14. Meka VG, Pillai SK, Sakoulas G, Wennersten C, Venkataraman L, DeGirolami PC, Eliopoulos GM, Moellering RC, Jr, Gold HS. 2004. Linezolid resistance in sequential Staphylococcus aureus isolates associated with a T2500A mutation in the 23S rRNA gene and loss of a single copy of rRNA. J Infect Dis 190:311–317. https://doi.org/10.1086/421471.
15. Long KS, Vester B. 2012. Resistance to linezolid caused by modifications at its binding site on the ribosome. Antimicrob Agents Chemother 56:603–612. https://doi.org/10.1128/AAC.05702-11.
16. Cidral TA, Carvalho MC, Figueiredo AM, de Melo MC. 2015. Emergence of methicillin-resistant coagulase-negative staphylococci resistant to linezolid with rRNA gene C2190T and G2603T mutations. APMIS 123:867–871. https://doi.org/10.1111/apm.12426.
17. Locke JB, Hilgers M, Shaw KJ. 2009. Mutations in ribosomal protein L3 are associated with oxazolidinone resistance in staphylococci of clinical origin. Antimicrob Agents Chemother 53:5275–5278. https://doi.org/10.1128/AAC.01032-09.
18. Klitgaard RN, Ntokou E, Nørgaard K, Biltoft D, Hansen LH, Trædholm NM, Kongsted J, Vester B. 2015. Mutations in the bacterial ribosomal protein l3 and their association with antibiotic resistance. Antimicrob Agents Chemother 59:3518–3528. https://doi.org/10.1128/AAC.00179-15.
19. Scheres SH. 2012. RELION: implementation of a Bayesian approach to cryo-EM structure determination. J Struct Biol 180:519–530. https://doi.org/10.1016/j.jsb.2012.09.006.
20. Cheng CY, Chou FC, Das R. 2015. Modeling complex RNA tertiary folds with Rosetta. Methods Enzymol 553:35–64. https://doi.org/10.1016/bs.mie.2014.10.051.
21. Phillips JC, Braun R, Wang W, Gumbart J, Tajkhorshid E, Villa E, Chipot C, Skeel RD, Kalé L, Schulten K. 2005. Scalable molecular dynamics with NAMD. J Comput Chem 26:1781–1802. https://doi.org/10.1002/jcc.20289.
22. Adams PD, Afonine PV, Bunkóczi G, Chen VB, Davis IW, Echols N, Headd JJ, Hung LW, Kapral GJ, Grosse-Kunstleve RW, McCoy AJ, Moriarty NW, Oeffner R, Read RJ, Richardson DC, Richardson JS, Terwilliger TC, Zwart PH. 2010. PHENIX: a comprehensive python-based system for macromolecular structure solution. Acta Crystallogr D Biol Crystallogr 66:213–221. https://doi.org/10.1107/S0907444909052925.
23. Khusainov I, Vicens Q, Bochler A, Grosse F, Myasnikov A, Ménétret JF, Chicher J, Marzi S, Romby P, Yusupova G, Yusupov M, Hashem Y. 2016. Structure of the 70S ribosome from human pathogen Staphylococcus aureus. Nucleic Acids Res 44:10491–10504. https://doi.org/10.1093/nar/gkw933.
24. Eyal Z, Matzov D, Krupkin M, Wekselman I, Paukner S, Zimmerman E, Rozenberg H, Bashan A, Yonath A. 2015. Structural insights into species-specific features of the ribosome from the pathogen Staphylococcus aureus. Proc Natl Acad Sci U S A 112:E5805–E5814. https://doi.org/10.1073/pnas.1517952112.
25. Schrodinger LLC. 2010. The PyMOL Molecular Graphics System, Version 1.3r1. Schrodinger LLC, New York, NY.
26. Pettersen EF, Goddard TD, Huang CC, Couch GS, Greenblatt DM, Meng EC, Ferrin TE. 2004. UCSF Chimera—a visualization system for exploratory research and analysis. J Comput Chem 25:1605–1612. https://doi.org/10.1002/jcc.20084.
27. Andrews JM. 2001. Determination of minimum inhibitory concentrations. J Antimicrob Chemother 48(Suppl 1):5–16. https://doi.org/10.1093/jac/48.suppl_1.5.
28. Belousoff MJ, Shapira T, Bashan A, Zimmerman E, Rozenberg H, Arakawa K, Kinashi H, Yonath A. 2011. Crystal structure of the synergistic antibiotic pair, lankamycin and lankacidin, in complex with the large ribosomal subunit. Proc Natl Acad Sci U S A 108:2717–2722. https://doi.org/10.1073/pnas.1019406108.
29. Murray RW, Melchior EP, Hagadorn JC, Marotti KR. 2001. Staphylococcus aureus cell extract transcription-translation assay: firefly luciferase reporter system for evaluating protein translation inhibitors. Antimicrob Agents Chemother 45:1900–1904. https://doi.org/10.1128/AAC.45.6.1900-1904.2001.
30. Leatherbarrow RJ. 2010. GraFit version 7, Erithacus Software Ltd., Horley, United Kingdom.
31. Novick RP. 1991. Genetic systems in staphylococci. Methods Enzymol 204:587–636.
32. Tang G, Peng L, Baldwin PR, Mann DS, Jiang W, Rees I, Ludtke SJ. 2007. EMAN2: an extensible image processing suite for electron microscopy. J Struct Biol 157:38–46. https://doi.org/10.1016/j.jsb.2006.05.009.
33. Li X, Mooney P, Zheng S, Booth CR, Braunfeld MB, Gubbens S, Agard DA, Cheng Y. 2013. Electron counting and beam-induced motion correction enable near-atomic-resolution single-particle cryo-EM. Nat Methods 10:584–590. https://doi.org/10.1038/nmeth.2472.
34. Mindell JA, Grigorieff N. 2003. Accurate determination of local defocus and specimen tilt in electron microscopy. J Struct Biol 142:334–347. https://doi.org/10.1016/S1047-8477(03)00069-8.
35. Li W, Liu Z, Koripella RK, Langlois R, Sanyal S, Frank J. 2015. Activation of GTP hydrolysis in mRNA-tRNA translocation by elongation factor G. Sci Adv 1:e1500169. https://doi.org/10.1126/sciadv.1500169.
36. Emsley P, Lohkamp B, Scott WG, Cowtan K. 2010. Features and development of coot. Acta Crystallogr D Biol Crystallogr 66:486–501. https://doi.org/10.1107/S0907444910007493.
37. Chan KY, Trabuco LG, Schreiner E, Schulten K. 2012. Cryo-electron microscopy modeling by the molecular dynamics flexible fitting method. Biopolymers 97:678–686. https://doi.org/10.1002/bip.22042.
38. Voorhees RM, Weixlbaumer A, Loakes D, Kelley AC, Ramakrishnan V. 2009. Insights into substrate stabilization from snapshots of the peptidyl transferase center of the intact 70S ribosome. Nat Struct Mol Biol 16:528–533. https://doi.org/10.1038/nsmb.1577.